Available online at www.sciencedirect.com
ScienceDirect
International Journal of Heat and Fluid Flow 27 (2006) 811–820
International Journal of HEAT AND FLUID FLOW
www.elsevier.com/locate/ijhff

# Large-eddy simulation of natural convection boundary layer on a vertical cylinder

D.G. Barhaghi [a,*], L. Davidson [a], R. Karlsson [a,b]

[a] Division of Fluid Dynamics, Department of Applied Mechanics, Chalmers University of Technology, SE-412 96 Göteborg, Sweden
[b] Vattenfall Utveckling AB, SE-814 26 Älvkarleby, Sweden

Received 30 September 2005; received in revised form 23 January 2006; accepted 4 March 2006
Available online 30 June 2006

**Abstract**

Large-eddy simulation of natural convection boundary layer along a constant temperature vertical cylinder is studied and the results are compared with experimental data. The highest local Grashof number is $Gr_z = 5 \times 10^{11}$. Although there are some discrepancies between the results in the region close to the wall, there is qualitative agreement between them. Mean values of the temperature near the wall show that the conventional law of the wall is valid in this case. However, the region where $\langle v^+ \rangle = r^+$, is much smaller than that of forced convection. With respect to turbulence production, the near-wall behavior of turbulent shear stress and normal stresses are investigated and compared with the experimental results. The existence of a negative shear stress region close to the wall in the simulations is confirmed and its influence on stream-wise normal stress is shown. The integral form of the momentum equation suggests that the buoyancy balances the combination of the turbulent stresses and the viscous term. The existence of a region where the energy spectra are proportional to $\kappa^{-3}$ is verified.


*Keywords:* Large-eddy simulation; LES; Natural convection; Free convection; Cylindrical coordinate system; Shell and tube; Boundary layer

## 1. Introduction

Natural convection is an interesting scientific subject in which many aspects need further research. The applications include not only industrial fields such as power generators, reactors, turbines, heat exchangers and other power conversion devices, but also natural phenomena such as atmospheric and oceanic currents, bio-heat transfer, greenhouse effects and heat transfer in stellar atmospheres.

Compared to the number of experimental and numerical studies that have been carried out in the field of forced convection heat transfer, few have been done in the field of natural convection. Among experimental researches, one is reported by Tsuji and Nagano (1988b). In that work, characteristics of natural convection boundary layer are compared with what has been reported in previous investigations. It is shown that the natural convection boundary layer has a unique turbulent structure that is rarely seen in other turbulent boundary layers. The results suggest that, for values of $y^+$ between 20 and 100, $\langle u'v' \rangle$ does not correlate with the mean velocity gradient, $\partial \langle u \rangle / \partial y$. Furthermore, a comparison of Reynolds shear stress distribution with observations in previous experiments showed a different behavior near the wall. Although no negative region was observed by Tsuji and Nagano (1988b), almost all previous works had shown a negative region close to the wall. They also show that the cross-correlation coefficient for shear stress ($R_{uv} = \langle u'v' \rangle / \sqrt{\langle u'^2 \rangle \times \langle v'^2 \rangle}$) becomes zero near the wall, which is in contradiction to analytical analysis.

Turbulent natural convection around a heated vertical slender cylinder was studied by Persson and Karlsson (1996) who presented new turbulent structures for the near-wall region. Again it was shown that there exists a negative shear stress region close to the wall. A comparison

* Corresponding author.
*E-mail address:* darioush@chalmers.se (D.G. Barhaghi).

0142-727X/$ - see front matter © 2006 Elsevier Inc. All rights reserved.
doi:10.1016/j.ijheatfluidflow.2006.03.009

of the normal stresses and temperature fluctuations with those proposed by Tsuji and Nagano (1988b) shows that the characteristics of the boundary layers are different between these two experiments. The temperature fluctuations presented by Tsuji and Nagano (1988b) are larger than the stream-wise normal stress while the reverse is seen in the work of Persson and Karlsson (1996). The location of the peaks remains in close agreement, however.

Natural convecting boundary layers have also been studied using DNS and LES. However, most of the studies include flows in either cavities or differentially heated channels. Among them are the researches conducted by Miki et al. (1993), Versteegh and Nieuwstadt (1998) and Peng and Davidson (2001).

Previous investigations have found that natural convection boundary layers still have many aspects that are not clear, and there are some other aspects in which there is no consensus. Furthermore very few researches have been conducted on the natural convective boundary layer along a vertical cylinder, and most of the studies have investigated flat plates, channels or horizontal cylinders. This and the existence of experimental apparatus at the Department of Applied Mechanics at Chalmers University of Technology gave the motivation to use LES to study the natural convection heat transfer along a vertical cylinder.

## 2. Geometry and grid setup

As shown in Fig. 1, a sector of a cylindrical concentric vertical shell and tube is adopted as the computational domain. All the dimensions are in millimeters. The motivation for using this geometry was an experimental equipment with almost the same dimensions at the Department of Applied Mechanics. This geometrical configuration was chosen because, although an idealized natural convecting boundary layer exists in infinite surroundings, it is nearly impossible to achieve such an ideal condition in either experiments or numerical calculations. Both experiments and calculations are very sensitive to the location of the infinite boundaries and any disturbances there. An inlet and outlet are designed to prevent stratification in the stagnant region that would affect the growth of the boundary layer near the hot tube.

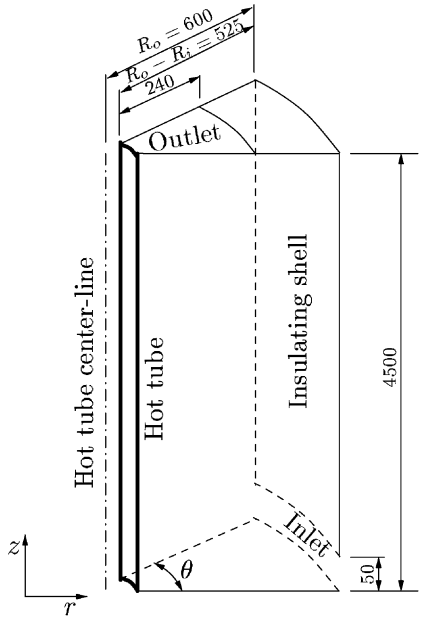


Fig. 1. Computational geometry. All dimensions in millimeter.

The span-wise extent of the geometry was chosen by comparing the results of different geometries. An ideal angle should cover all turbulent structures and give averaged two-dimensional angle-independent results. In this work, different angles, $\theta = 18°$, 36°, 54°, 72° and 90°, are studied.

Having studied the flow in different grid sizes, a $98 \times 402 \times 162$ grid ($r$, $z$ and $\theta$ directions) with $\theta = 90°$ was finally chosen.

Different grid densities were applied at the inlet in the $z$-direction as compared to the rest of the domain. The inlet is covered by 18 cells, each of which is $\Delta z \approx 2.78$ mm. From the inlet up to $z = 170$ mm, the grid is stretched by approximately 9%. An equidistant mesh with $\Delta z \approx 11.9$ mm is used from this height up to the top of the geometry.

The spatial resolution along the hot cylinder is $\Delta\theta^+ < 3.5$ in the span-wise direction and $\Delta z^+ < 55$ in the stream-wise direction. The maximum non-dimensional distance between cylinder adjacent nodes and the cylinder is $r^+ = 0.32$. It is found that the maximum SGS viscosity ($\nu_t$) in the boundary layer is less than 50% of the fluid viscosity and in the region $r^+ < 100$, it is less than 10% of the fluid viscosity. This indicates that the boundary layer is very well resolved (see Barhaghi, 2004).

## 3. Numerical method

### 3.1. Governing equations

The incompressible continuity, Navier–Stokes and energy equations in cylindrical coordinate system are solved. The Boussinesq approximation is employed for the buoyancy term in the vertical momentum equation. The Smagorinsky model is used to model the sub-grid scales. In the momentum equations, the turbulent diffusive cross terms arising from $\frac{\partial}{\partial x_j}\left(\nu_{\text{eff}}\frac{\partial\langle v_j\rangle}{\partial x_i}\right)$ are neglected.

### 3.2. Finite volume approach

A conventional finite volume method (Versteegh and Malalasekera, 1995) is used to solve the governing equations. As it is very important not to dissipate the turbulence by conventional numerical schemes, it is customary to discretize the governing equations by central difference scheme. This approach, however, causes a so called unphysical fluctuation or wiggle problem which is related to the unboundedness of the central difference scheme. This

problem can especially be encountered in regions where turbulence intensity is not sufficiently high or in laminar regions and regions where the grid is not sufficiently fine. Both problems occur in the present LES simulations near the inlet. Using a pure central difference scheme, these unphysical fluctuations were generated near the inlet and propagated throughout the computational domain. To remedy this problem, a blend of central difference scheme with deferred correction (Ferziger and Peric, 1996) and the Van-Leer scheme was used (Dahlström and Davidson, 2003).

The second-order Crank–Nicolson scheme was used to discretize the equations in time. The numerical procedure is based on an implicit, fractional step technique with a multi-grid pressure Poisson solver (Emvin, 1997) and a non-staggered grid arrangement (Davidson and Peng, 2003).

### 3.3. Boundary conditions and fluid data

Simulation of laminar regions with the LES method may provoke the problem of unphysical fluctuations. To create turbulence at the inlet, the velocity field of the DNS of a channel flow was scaled such that the bulk velocity became 0.6 m/s and was implemented as an inlet boundary condition for velocities. A no-slip boundary condition is used for all solid boundaries.

For the temperature, the Dirichlet boundary condition was applied at the hot tube and the inlet. The temperature was set to 80 °C and 25 °C at the hot tube and at the inlet, respectively. Except for the outlet, a homogeneous Neumann boundary condition was used over all the remaining boundaries.

A convective boundary condition (Sohankar et al., 1998) was applied at the outlet for both temperature and velocities.

The fluid dynamic viscosity and the laminar and turbulent Prandtl numbers are $\mu = 18.9 \times 10^{-6}$, $Pr = 0.7$ and $Pr_t = 0.4$, respectively.

To accelerate the convergence of the numerical computations to a fully developed condition, either the results of a 2D-RANS simulation or the results of previous simulations for different grid configurations were interpolated and applied as initial boundary conditions.

## 4. Results

Once the fully developed condition is achieved, sampling can be started. Sampling should last sufficiently long to ensure time-independent results. This is checked by comparing two different averaged results with a different number of samples.

### 4.1. Fully developed flow assessment

The instantaneous local Nusselt number at different heights was calculated to assess whether the flow has become fully developed so that sampling can be started. The instantaneous, filtered and averaged Nusselt numbers are shown in Fig. 2 for two vertical levels, one near the inlet and one near the outlet. It can be observed that Nusselt numbers fluctuate uniformly for almost the last 15,000 time steps. The filtered value, which is an average of 2000 instantaneous neighboring Nusselt numbers, shows this more clearly. These figures verify that the flow has reached a fully developed state and the statistical averaging can be started.

Fig. 3 shows velocity and Reynolds shear stress obtained from the last three 5000 time steps of simulation. As can be seen, there is very little difference between the results. For the shear stress, the largest difference lies in the outer region near the outer shell, far from the boundary layer. Again, in these two figures, it can be seen that the simulation has reached the fully developed state. Hereafter, the statistics and averaged values are calculated using the last 15,000 time steps.

### 4.2. Grid-independent result

A grid-independent result is always desirable in numerical simulations. This can be checked by comparing the results of different grids. However, as LES is inherently

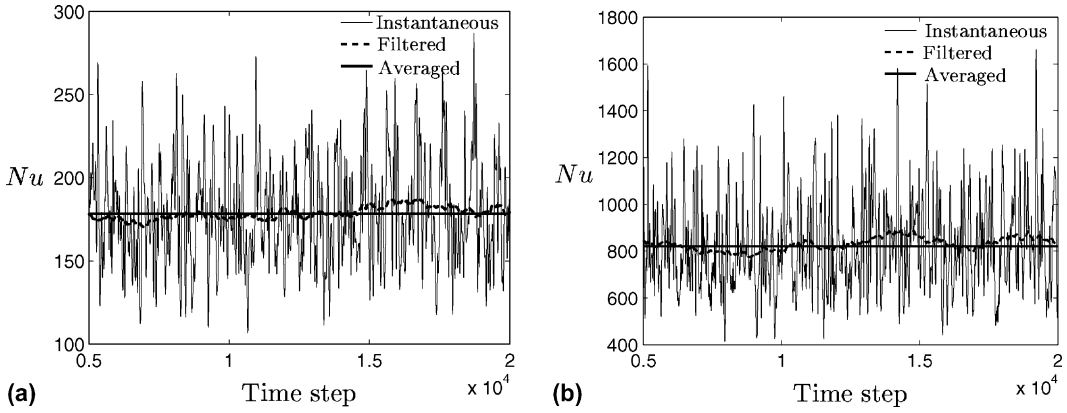


Fig. 2. Assessment of fully developed flow as regards the local Nusselt number: (a) $z/H = 0.2$ and (b) $z/H = 0.9$.

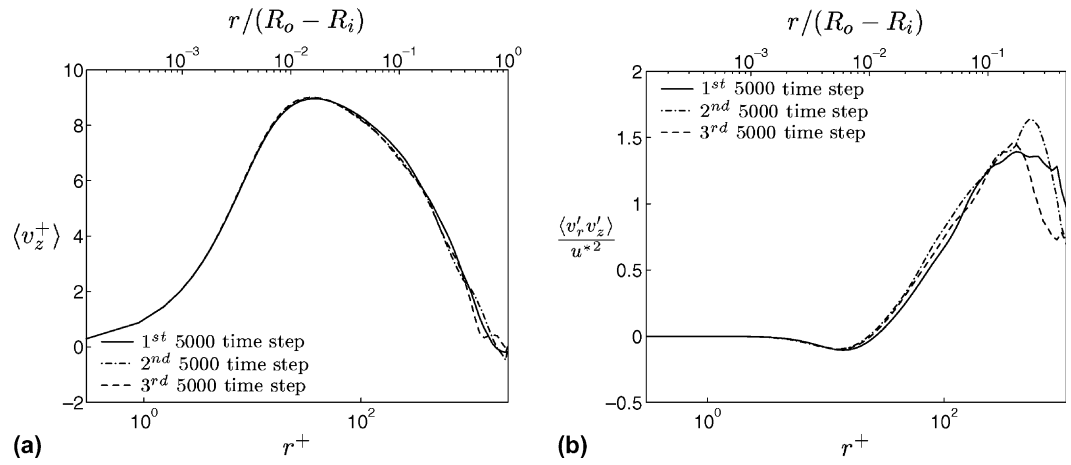


Fig. 3. Velocity and shear stress at $z/H = 0.8$, $Gr = 2.9 \times 10^{11}$ for contiguous averaged data: (a) dimensionless velocity and (b) Reynolds shear stress.

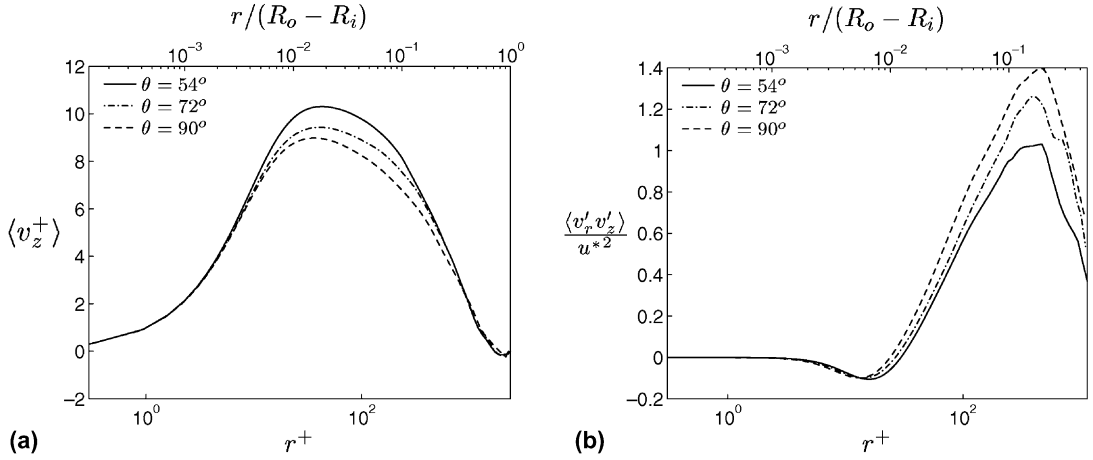


Fig. 4. Velocity and shear stress at $z/H = 0.8$, $Gr_z = 2.9 \times 10^{11}$ for different domains: (a) dimensionless velocity and (b) Reynolds shear stress.

dependent on the grid resolution, no final grid-independent result exists. In these computations, a final $98 \times 402$ mesh in the $r$- and $z$-directions is chosen. However it is found that the angular width of the domain has a crucial effect on the final results. This is shown in Fig. 4 which depicts velocity and shear stress for different sizes of the computational domain.

Although the grid spacing in the $\theta$-direction is the same for all grids, it can be seen that the difference between the curves for $\theta = 72°$ and $\theta = 90°$ is less than that for $\theta = 54°$ and $\theta = 72°$, both for velocity and shear stress. Although it is not shown, the difference between the results of other grids with $\theta = 18°$, $\theta = 36°$ was even larger. As can be seen in Fig. 5, the difference between the Nusselt numbers for geometries with $\theta = 72°$ and $\theta = 90°$ is smaller than the difference between $\theta = 54°$ and $\theta = 72°$.

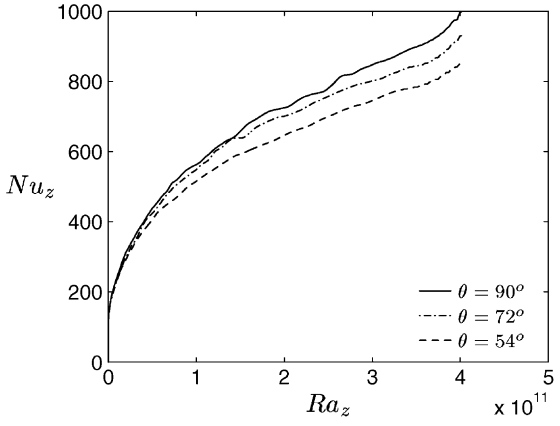


Fig. 5. Nusselt number at $z/H = 0.9$, $Gr_z = 4.2 \times 10^{11}$ for different domains.

### 4.3. Mean fluid flow and heat transfer parameters

Fig. 6(a) and (b) compare the results of the present study and previous experiments. The predicted profiles were obtained by averaging over $\theta$ and $t$ (time). As can be seen, although the results of the present study are in good agreement with the results of Tsuji and Nagano (1988a), the results of Persson and Karlsson (1996) are rather different.

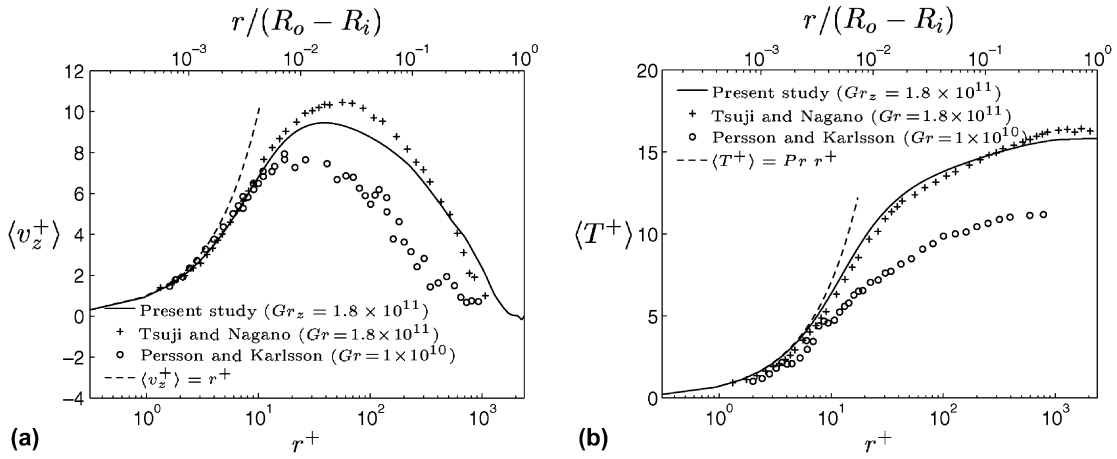


Fig. 6. Comparison of velocity and temperature with experimental data: (a) dimensionless velocity and (b) dimensionless temperature.

A common behavior in all graphs, however, except for a very small distance from the wall, $r^+ < 1.2$, is that the velocity does not follow the law of the wall, $\langle v_z^+ \rangle = r^+$, in the same way as it does for forced convecting boundary layers. However, Fig. 6(b) shows that temperature follows the law of the wall in the region $r^+ < 5$, similar to forced convecting flows.

Although no self-similar behavior with respect to dimensionless velocity $\langle v_z^+ \rangle$ could be observed in the results of Tsuji and Nagano (1988a), graphs of the $\langle v_z^+ \rangle$ vs. $r^+$ in this study collapse on each other, showing self-similar behavior, see Fig. 7.

Finally, Fig. 8 shows the variation of the Nusselt number as a function of the Rayleigh number. Compared to the results of Tsuji and Nagano (1988a) and the proposed correlation for the laminar region, there is very good agreement for both the laminar and the turbulent region. The major difference is in the transition region. The transition in the LES simulations starts at $Ra_z = 10^6$, as compared to the flow along the flat plate, for which transition starts at $Ra = 8 \times 10^8$. The difference may be due to any or a combination of three factors: first, in this cylindrical cavity, the flow at the inlet is turbulent; second, there might be

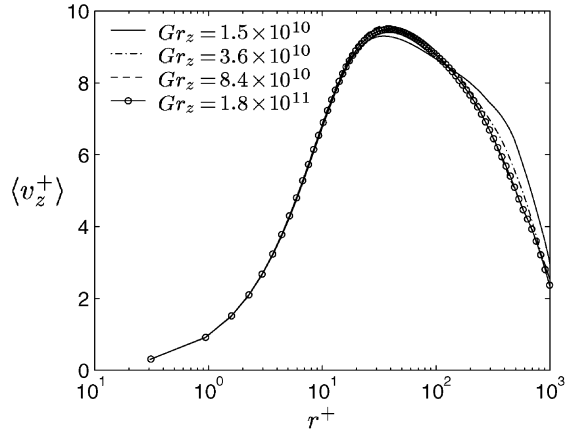


Fig. 7. Dimensionless velocity profiles at different Grashof numbers.

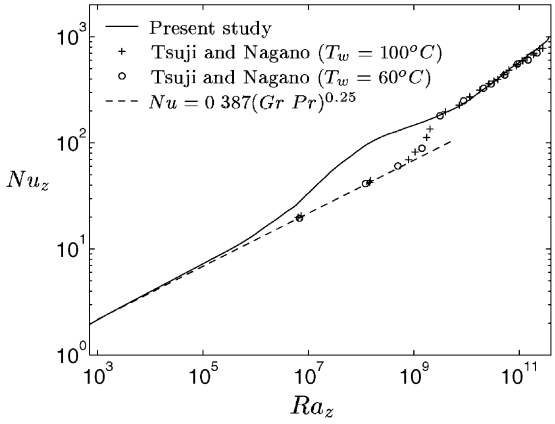


Fig. 8. Nusselt number as a function of Rayleigh number.

inherent differences between the characteristics of a boundary layer along a vertical flat plat and a vertical slender cylinder; and third, there is an outer shell that embraces the whole cylinder and provokes instabilities by creating some recirculating flows in the proximity of the boundary layer.

Another difference in Fig. 8 is the overshoot of the Nusselt number in the commencement of the turbulent boundary layer ($Ra_z \approx 10^8$), which was not observed by Tsuji and Nagano (1988a) but had been mentioned in previous researches (e.g. Cheesewright, 1968).

### 4.4. Reynolds stresses and turbulent heat fluxes

Fig. 9 compares the computed normal stresses and temperature fluctuations with the experimental data. In Fig. 9(a), both the predicted $\sqrt{\langle t't' \rangle}/t^*$ and the stream-wise normal stress have higher values than the experimental data for the flat plate. The wall-normal stress, however, has smaller values for $r^+ < 92.5$. No constant value region such as that observed in the experiment for $\sqrt{\langle v_r'^2 \rangle}/u^*$ in the $7.5 < r^+ < 40$ region can be observed in the LES simulations. Nevertheless, the graphs are qualitatively in a good agreement and the locations of maxima match each other.

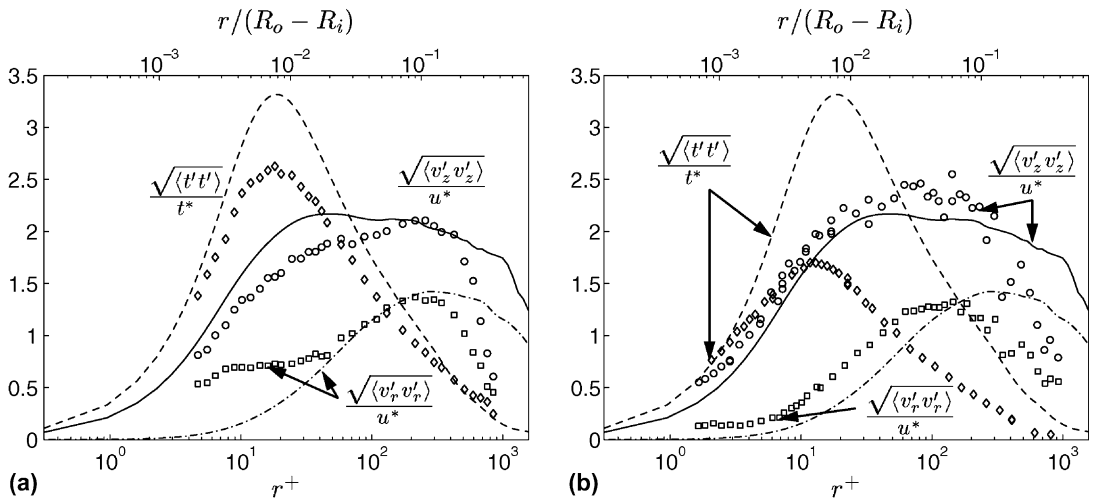


Fig. 9. Normal stresses and temperature fluctuations. Lines: simulation, $Gr_z = 8.9 \times 10^{10}$ ($z/H = 0.5$); markers: experiments: (a) experimental data from Tsuji and Nagano (1988b), $Gr = 8.99 \times 10^{10}$ and (b) experimental data from Persson and Karlsson (1996), $Gr = 1 \times 10^{10}$.

Discrepancies between experiments and computations are even larger in Fig. 9(b). Contrary to computations and the other experimental data, normalized temperature fluctuations in the experiment are smaller than the stream-wise velocity fluctuations. Furthermore, the locations of maxima are too close to the wall.

Experimental wall-normal stress in Fig. 9(b) shows the same behavior as computations, in contrast to that presented by Tsuji and Nagano (1988a). However, none of the experiments show a tendency for this parameter to become zero sufficiently close to the wall, reflecting the unreliability of measurements close to the wall.

Reynolds shear stress together with stream-wise and wall-normal turbulent heat fluxes are shown in Fig. 10. Again, although the computed values in Fig. 10(a) are in close agreement with the experimental results, this is not the case in Fig. 10(b). While wall-normal turbulent heat flux remains positive close to the wall for both computations and experiments in Fig. 10(a), it takes negative values for the experiment shown in Fig. 10(b). Also contrary to the computations and experiment shown in Fig. 10(b), no negative shear stress can be observed in the experimental values shown in Fig. 10(a). This behavior is similar to the case of natural convection boundary layer in an infinite channel where the turbulent shear stress remains positive across the walls (see Barhaghi (2004) and Versteegh and Nieuwstadt (1998)). However one significant difference between these two boundary layers is that the convective terms are zero in case of infinite channel.

In the experiment of Persson and Karlsson (1996), no negative region can be observed close to the wall for stream-wise turbulent heat flux, albeit that the existence of this region was confirmed by Tsuji and Nagano (1988b).

As mentioned earlier, the computed locations at which stresses are maximum are in reasonably good agreement with the experimental values of Tsuji and Nagano

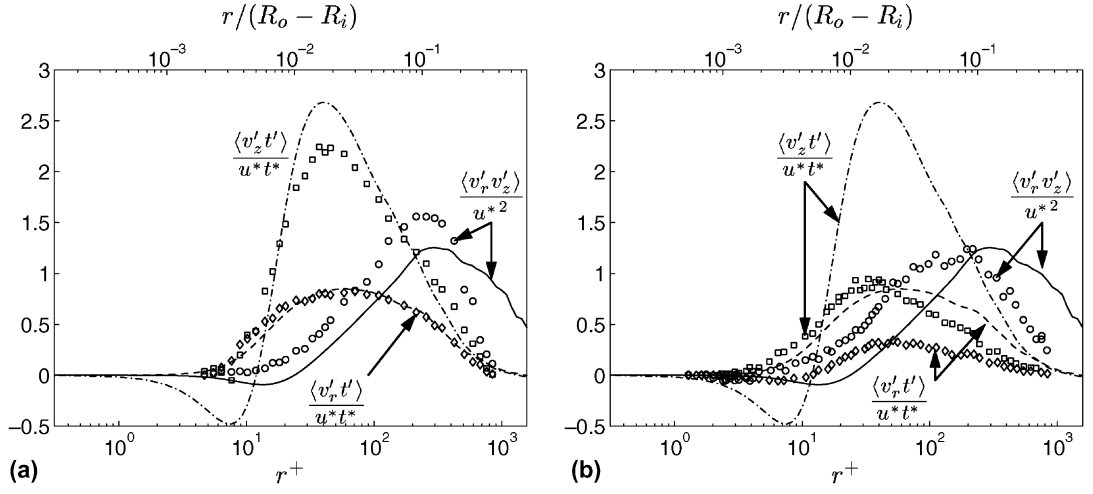


Fig. 10. Turbulent shear stress and heat fluxes. Lines: simulation, $Gr_z = 8.9 \times 10^{10}$; markers: experiments: (a) experimental data from Tsuji and Nagano (1988b), $Gr = 8.99 \times 10^{10}$ and (b) experimental data from Persson and Karlsson (1996), $Gr = 2 \times 10^{10}$.

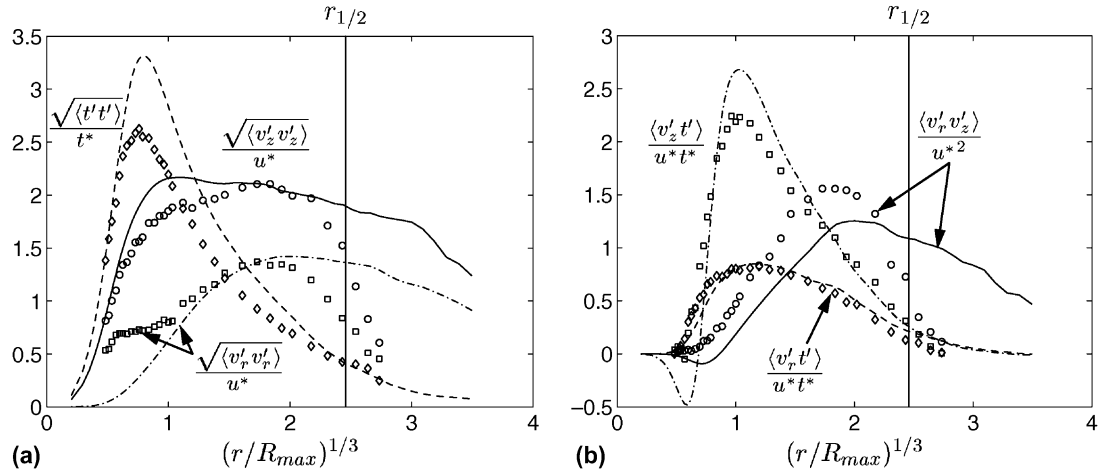


Fig. 11. Reynolds stresses and turbulent heat fluxes as a function of the distance from the hot tube and the location of the maximum boundary layer velocity. Lines: simulation, $Gr_z = 8.9 \times 10^{10}$; markers: experimental data from Tsuji and Nagano (1988b), $Gr = 8.99 \times 10^{10}$: (a) normal stresses and temperature fluctuations and (b) shear stress and turbulent heat fluxes.

(1988b). This can be observed more clearly in Fig. 11, in which $R_{\max}$ is the location of the maximum velocity of the boundary layer. The thick vertical line represents the location of $r_{1/2}$ at which the velocity is half of the boundary layer maximum velocity. It is defined as the natural convection boundary layer thickness.

It can be observed in Fig. 11 that the maximum values of $\langle t't'\rangle$, $\langle v_z't'\rangle$ and $\langle v_r't'\rangle$ lie close to the location of the maximum velocity. However, the maximum values of $\sqrt{\langle v_r'v_r'\rangle}$, and $\sqrt{\langle v_z'v_z'\rangle}$ in the experiment as well, lie far from the location of maximum velocity in the outer part of the boundary layer. This is claimed to be the characteristic difference between the natural convection and forced convection boundary layers (e.g. Tsuji and Nagano (1988b)). In forced convection boundary layers, it is observed that the location of the maximum of all fluctuations is close to the location of the maximum velocity.

However, the negative turbulent shear stress ($\langle v_r'v_z'\rangle$) close to the wall in the simulations gives a more flat profile of $\langle v_z'v_z'\rangle$. This effect can be investigated by considering the production term in the $\langle v_z'v_z'\rangle$-equation, which reads:

$$P_{zz} = -2\langle v_r'v_z'\rangle \frac{\partial\langle v_z\rangle}{\partial r} - 2\langle v_z'v_z'\rangle \frac{\partial\langle v_z\rangle}{\partial z} + 2g_z\beta\langle v_z't'\rangle$$

Each of the terms in the above equation, together with the summation of all terms normalized by $u^{*3}$, are plotted in Fig. 12. As expected, the production arising from stream-wise velocity fluctuations is negligible as compared to the production of turbulence by turbulent shear stress ($-2\langle v_r'v_z'\rangle\partial\langle v_z\rangle/\partial r$) and buoyancy ($2g_z\beta\langle v_z't'\rangle$). As can be observed, both the experiment and the simulation show a negative value for stream-wise turbulent heat transfer, resulting in a negative buoyancy production near the hot tube. As the stream-wise turbulent heat transfer, $\langle v_z't'\rangle$, changes sign, the production term due to buoyancy changes to a positive sign and attains its maximum at the location of the maximum $\langle v_z't'\rangle$, which is close to the location of the maximum boundary layer velocity. This term diminishes when approaching the outer part of the boundary layer as $\langle v_z't'\rangle$ diminishes. However, the major difference between the experiment and the simulation is in the existence of the negative turbulent shear stress, $\langle v_r'v_z'\rangle$. Since near the wall, the gradient of the velocity is positive and turbulent shear stress is negative, the $-2\langle v_r'v'z\rangle\partial\langle v_z\rangle/\partial r$ term becomes positive, resulting in a large production of turbulence, which is in contradiction to the experiment of Tsuji and Nagano (1988b). In the experiment, the existence of a small positive turbulent shear stress region close to the wall up to the location of the maximum velocity, where the velocity gradient and consequently production due to shear stress are zero, suggests a rather small negative value for the production of turbulence by turbulent shear stress, i.e. $-2\langle v_r'v_z'\rangle\partial\langle v_z\rangle/\partial r$, in the inner part of the boundary layer. The summation of the two negative production terms causes a large negative $P_{zz}$ in the major portion of the inner

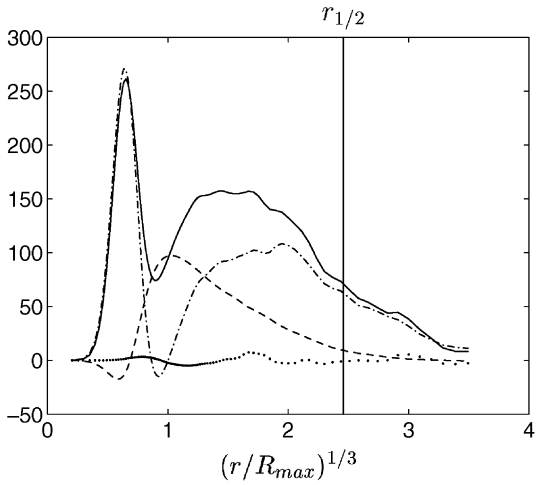


Fig. 12. Turbulence production term in $\langle v'_z v'_z\rangle$-equation. (—) $P_{zz}$; (–·–) $-2\langle v_r'v_z'\rangle\partial\langle v_z\rangle/\partial r$; (- - -) $2g_z\beta\langle v_z't'\rangle$; (···) $-2\langle v_z'v_z'\rangle\partial\langle v_z\rangle/\partial z$.

part of the boundary layer. $P_{zz}$ in both the experiment and the simulation behaves similarly almost from the location of the maximum velocity toward the edge of the boundary layer where $\partial\langle v_z\rangle/\partial r < 0$ and $\langle v_r' v_z'\rangle > 0$. Although the variation in the total production across the boundary layer in the simulation agrees well with the behavior of the stream-wise velocity fluctuations, this is not observed in the experiment, in which the existence of negative or small positive production of turbulence in the inner part of the boundary layer, where $v_z \leqslant v_{\max}$, does not quite hold with the large values of $\langle v_z' v_z'\rangle$ in Fig. 11(a), suggesting that there should be a region of negative shear stress in the experimental results.

Another difference between the experimental and simulation results can be found by considering the production term in the $\langle v_r' v_z'\rangle$-equation, which reads:

$$P_{rz} = -\langle v_r' v_r'\rangle \frac{\partial\langle v_z\rangle}{\partial r} - \langle v_r' v_r'\rangle \frac{\partial\langle v_z\rangle}{\partial z} - \langle v_r' v_z'\rangle \frac{\partial\langle v_r\rangle}{\partial r} - \langle v_z' v_z'\rangle \frac{\partial\langle v_r\rangle}{\partial z} + g_z\beta\langle v_r' t'\rangle$$

Fig. 13 shows the variation in $P_{rz}$ and each separate term of the above equation across the boundary layer. All the terms are normalized by $u^{*3}$. As expected, all the terms except the production resulting from the wall-normal velocity fluctuations, $-\langle v_r' v_r'\rangle\partial\langle v_z\rangle/\partial r$, and buoyancy production due to wall-normal turbulent heat flux, $g_z\beta\langle v_r' t'\rangle$, are negligible. Fig. 13 shows that, close to the wall, in the inner part of the boundary layer, the production due to buoyancy is smaller than the production due to $\langle v_r' v_r'\rangle$ resulting in negative total production. On the other hand, in the experimental results of Tsuji and Nagano (1988b), with respect to Fig. 10(a), it can be concluded that, owing to the good agreement between wall-normal turbulent heat fluxes in the simulation and experiment, the amount of production caused by buoyancy in the experiment is equal to that in the simulation. In the experiment, however, owing to the larger values of $\langle v_r' v_r'\rangle$ near the wall (see Fig. 10(a)), the magnitude of $\langle v_r' v_r'\rangle\partial\langle v_z\rangle/\partial r$ will be larger than that in the simulation, resulting in larger negative $P_{rz}$, again suggesting that a region of negative turbulent shear stress should exist.

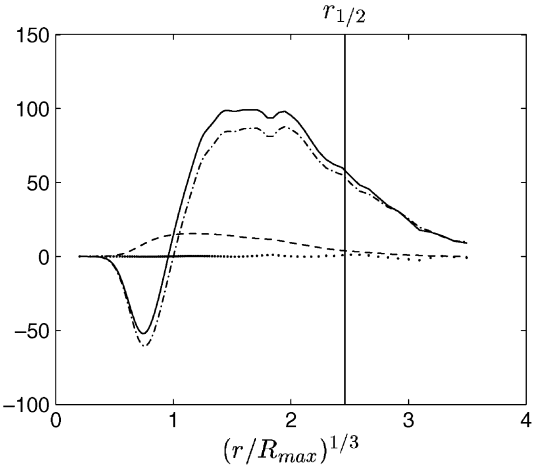


Fig. 13. Turbulence production term in $\langle v'_r v'_z\rangle$-equation. (—) $P_{rz}$; (–·–) $-\langle v_r' v_r'\rangle\partial\langle v_z\rangle/\partial r$; (- - -) $g_z\beta\langle v_r' t'\rangle$; (···) $-\langle v_r' v_z'\rangle\partial\langle v_z\rangle/\partial z - \langle v_r' v_z'\rangle\partial\langle v_r\rangle/\partial r - \langle v_z' v_z'\rangle\partial\langle v_r\rangle/\partial z$.

Fig. 14 shows the integral form of the vertical momentum and the temperature equations. As shown in Tsuji and Nagano (1988b) and in Fig. 14, the pressure term does not play a vital role in the balance of the stream-wise velocity. Also it can be noticed that, although the impact of the negative shear stress is considerable in the behavior of the turbulence near the wall, the magnitude of the negative shear stress is so small that it is difficult to detect it in Fig. 14(a). The shear stress has an almost negligible effect on the mean values of the flow close to the wall. Terms in this figure are denoted as shown in Eqs. (1) and (2).

$$\begin{aligned}\langle v_z\rangle \text{ Balance} = &\overbrace{-\int_{R_i}^{r}\left[\frac{1}{r}\frac{\partial}{\partial r}(r\langle v_r\rangle\langle v_z\rangle)+\frac{\partial}{\partial z}(\langle v_z\rangle^2)\right]r\,\mathrm{d}r}^{\text{AT}}\\ &+\overbrace{\int_0^r g\beta(\langle T\rangle - T_{\text{ref}})r\,\mathrm{d}r}^{\text{BT}}\\ &+\underbrace{\int_{R_i}^{r}\left[\frac{1}{r}\frac{\partial}{\partial r}\left(r\nu_{\text{eff},v}\frac{\partial\langle v_z\rangle}{\partial r}\right)+\frac{\partial}{\partial z}\left(\nu_{\text{eff},v}\frac{\partial\langle v_z\rangle}{\partial z}\right)\right]r\,\mathrm{d}r}_{\text{VT}}\\ &-\underbrace{\int_{R_i}^{r}\left[\frac{1}{r}\frac{\partial}{\partial r}(r\langle v_r' v_z'\rangle)+\frac{\partial}{\partial z}\langle v_z' v_z'\rangle\right]r\,\mathrm{d}r}_{\text{FT}}\\ &-\underbrace{\int_{R_i}^{r}\frac{1}{\rho}\frac{\partial\langle p\rangle}{\partial z}r\,\mathrm{d}r}_{\text{PT}}\end{aligned} \tag{1}$$

$$\begin{aligned}\langle T\rangle \text{ Balance} = &\overbrace{-\int_{R_i}^{r}\left[\frac{1}{r}\frac{\partial}{\partial r}(r\langle v_r\rangle\langle T\rangle)+\frac{\partial}{\partial z}(\langle v_z\rangle\langle T\rangle)\right]r\,\mathrm{d}r}^{\text{AT}}\\ &+\underbrace{\int_{R_i}^{r}\left[\frac{1}{r}\frac{\partial}{\partial r}\left(r\nu_{\text{eff},T}\frac{\partial\langle T\rangle}{\partial r}\right)+\frac{\partial}{\partial z}\left(\nu_{\text{eff},T}\frac{\partial\langle T\rangle}{\partial z}\right)\right]r\,\mathrm{d}r}_{\text{CT}}\\ &-\underbrace{\int_{R_i}^{r}\left[\frac{1}{r}\frac{\partial}{\partial r}(r\langle v_r' t'\rangle)+\frac{\partial}{\partial z}\langle v_z' t'\rangle\right]r\,\mathrm{d}r}_{\text{FT}}\end{aligned} \tag{2}$$

Investigation of Fig. 14(a) yields that as the maximum velocity location is approached ($r^+ = 37$), the viscous diffusion term (VT) attains its maximum that is equal to wall shear force per unit length. $R_i\Theta \times \tau_w = R_i\Theta \times \nu\partial\langle v_z\rangle/\partial r|_{r=R_i}$, and remains constant. Consequently, the fluctuating term (FT), to which the shear stress mainly contributes, increases and, together with the wall shear stress, $\tau_w$, balances the buoyancy term (BT). The advective term (AT) is almost negligible in the entire velocity boundary layer. However, it achieves considerable values near the edge of the boundary layer in the temperature equation. In contrast to the momentum equation, there is no buoyancy term in the energy equation. Therefore the fluctuating

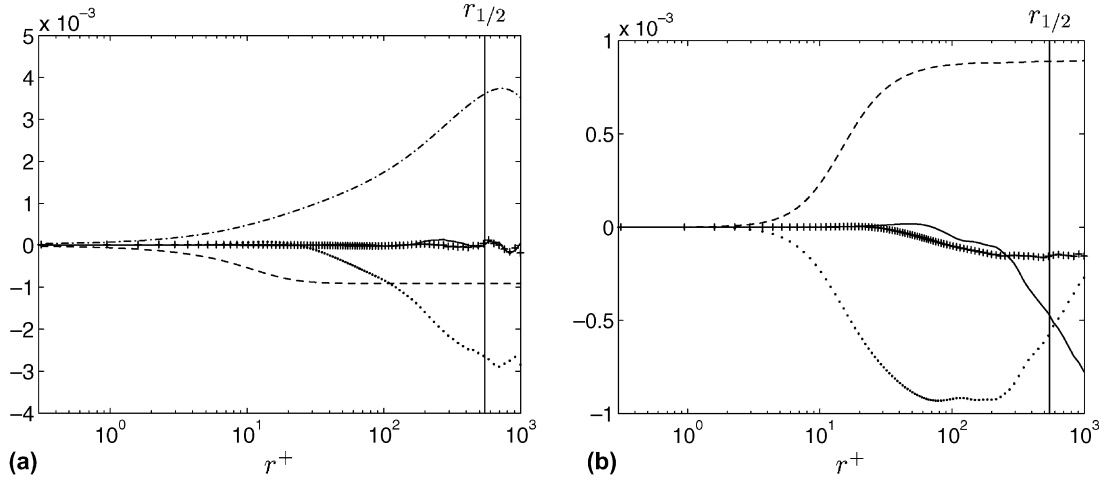


Fig. 14. Integral form of the $z$-momentum and temperature equations at $Gr_z = 8.9 \times 10^{10}$. (—) AT; (–·–) BT; (---) VT or CT; ··· FT; (+) Balance: (a) $v_z$-equation and (b) temperature equation.

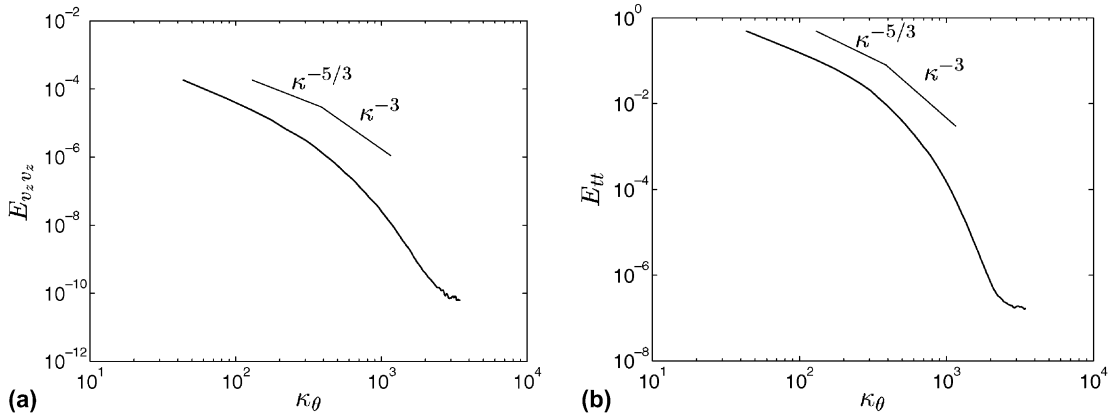


Fig. 15. One-dimensional energy spectra variation in the span-wise (cyclic) direction at $r^+ = 59$, $Gr_z = 1.8 \times 10^{11}$ ($z/H = 0.7$): (a) axial velocity energy spectrum and (b) temperature energy spectrum.

terms here balance the conductive terms. This is one reason why the wall-normal turbulent heat flux reaches its maximum in the inner part of the boundary layer. It should be mentioned here that the contribution of the stream-wise turbulent heat flux to Eq. (2) is almost negligible.

Energy spectra for velocity and temperature fluctuations in a region close to the wall are shown in Fig. 15. As can be seen in the figure, the cut-off has taken place well beyond the range where energy spectra are proportional to $\kappa^{-3}$. This is a region that is believed to immediately follow the inertial subrange, where $E \propto \kappa^{-5/3}$ (e.g. Peng and Davidson (2002)).

Finally, Fig. 16 compares the cross correlation coefficient of the shear stress. From Taylor expansion, $\langle v_r' v_z' \rangle = \mathcal{O}(r^3)$, $\langle v_r'^2 \rangle = \mathcal{O}(r^4)$ and $\langle v_z'^2 \rangle = \mathcal{O}(r^2)$. Thus $R_{uv}$ should have a constant value very close to the wall when $r$ approaches zero. This can be found in Fig. 16 for the present simulation and Persson and Karlsson (1996), for which the constant values are $R_{uv} \approx -0.3$ and $R_{uv} \approx -0.09$, respectively. As this coefficient becomes zero in the experiment of Tsuji and Nagano (1988a), it can again be deduced that the measured stresses for this experiment are unreliable in the region close to the wall.

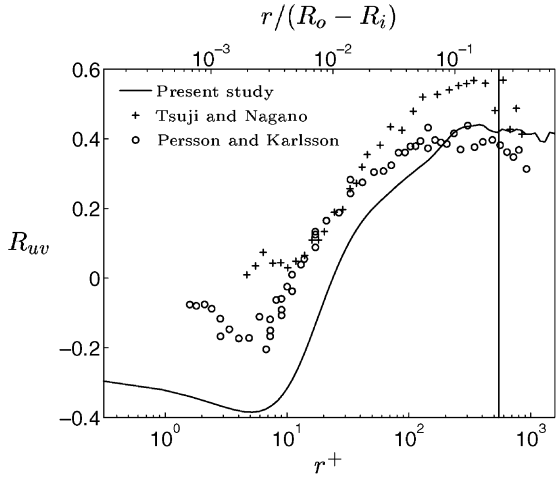


Fig. 16. Cross correlation coefficient, $R_{uv} = \langle v_r' v_z' \rangle / \sqrt{\langle v_r'^2 \rangle \times \langle v_z'^2 \rangle}$; comparison at $Gr_z = 8.9 \times 10^{10}$ ($z/H = 0.5$).

## 5. Conclusions

Natural convection boundary layer along a constant temperature vertical cylinder is studied. As it was postulated by Tsuji and Nagano (1988a), the existence of a narrow region close to the wall, $r^+ < 1.2$, where the linear law of the wall for the velocity holds, is verified. The profiles of the velocity collapse on each other in the turbulent region, showing a self-similar behavior.

The Nusselt number is compared with experimental values and it is deduced that the transition for this simulation has started earlier as compared to experiments on the vertical wall. The simulations exhibit an overshoot in the commencement of the turbulent region.

Comparison of the calculated Reynolds stresses with those obtained from experiments suggests different boundary layer behaviors. To clarify these differences, further investigations are desirable. However, the discontinuous behavior of the cross correlation coefficient in case of Tsuji and Nagano (1988a), leaves a question on the accuracy of the measured Reynolds stresses near the wall.

In the present computations, a small region in the inner layer of the boundary layer is found where the turbulent shear stress attains negative values. The location of the maximum magnitude of the negative shear stress lies at $(r/R_{\max})^{1/3} \approx 0.75$. Although this is not in agreement with the results of Tsuji and Nagano (1988a) and Tsuji and Nagano (1988b), by considering the works of Ampofo and Karayiannis (2003) and Paolucci (1990), there exist such a small region in the vicinity of wall. As there is no such region in case of natural convection boundary layer in an infinite channel (Barhaghi (2004) and Versteegh and Nieuwstadt (1998)) where the boundary layer is fully developed, the reason for the existence of such region in the developing natural convection boundary layers is probably related to the convective terms that are zero in case of non-developing boundary layers.

## Acknowledgements

The financial support of the Swedish Research Council and computer resources provided by the Center for Parallel Computing (PDC), KTH, are greatly acknowledged. The authors are also indebted to Dr. Shia-Hui Peng for his support and for sharing his ideas and knowledge.

## References

Ampofo, F., Karayiannis, T.G., 2003. Experimental benchmark data for turbulent natural convection in an air filled square cavity. International Journal of Heat and Mass Transfer 46, 3551–3572.

Barhaghi, D.G., 2004. DNS and LES of turbulent natural convection boundary layer. Thesis for Licentiate of Engineering 04/05, Department of Thermo and Fluid Dynamics, Chalmers University of Technology, Göteborg, Sweden.

Cheesewright, R., 1968. Turbulent natural convection from a plane vertical surface. Journal of Heat Transfer 90, 1–8.

Dahlström, S., Davidson, L., 2003. Large eddy simulation applied to a high-reynolds flow around an airfoil close to stall. AIAA Paper, 2003-0776.

Davidson, L., Peng, S.-H., 2003. Hybrid LES-RANS: a one-equation SGS model combined with a $k-\omega$ model for predicting recirculating flows. International Journal for Numerical Methods in Fluids 43, 1003–1018.

Emvin, P., 1997. The full multigrid method applied to turbulent flow in ventilated enclosures using structured and unstructured grids. Ph.D. thesis, Department of Thermo and Fluid Dynamics, Chalmers University of Technology, Göteborg.

Ferziger, J.H., Peric, M., 1996. Computational Methods for Fluid Dynamics. Springer-Verlag, Berlin.

Miki, Y., Fukuda, K., Taniguchi, N., 1993. Large eddy simulation of turbulent natural convection in concentric horizontal annuli. International Journal of Heat and Fluid Flow 14, 210–216.

Paolucci, S., 1990. Direct numerical simulation of two-dimensional turbulent natural convection in an enclosed cavity. Journal of Fluid Mechanics 215, 229–262.

Peng, S.-H., Davidson, L., 2001. Large eddy simulation for turbulent buoyant flow in a confined cavity. International Journal of Heat and Fluid Flow 22, 323–331.

Peng, S.-H., Davidson, L., 2002. On a subgrid-scale heat flux model for large eddy simulation of turbulent thermal flow. International Journal of Heat and Mass Transfer 45, 1393–1405.

Persson, N.J., Karlsson, R.I., 1996. Turbulent natural convection around a heated vertical slender cylinder. In: 8th Int. Symp. on Applications of Laser Techniques to Fluid Mechanics. Lisbon.

Sohankar, A., Norberg, C., Davidson, L., 1998. Low-Reynolds number flow around a square cylinder at incidence: study of blockage, onset of vortex shedding and outlet boundary condition. International Journal for Numerical Methods in Fluids 26, 39–56.

Tsuji, T., Nagano, Y., 1988a. Characteristics of a turbulent natural convection boundary layer along a vertical flat plate. International Journal of Heat and Mass Transfer 31 (8), 1723–1734.

Tsuji, T., Nagano, Y., 1988b. Turbulence measurements in a natural convection boundary layer along a vertical flat plate. International Journal of Heat and Mass Transfer 31 (10), 2101–2111.

Versteegh, H.K., Malalasekera, W., 1995. An Introduction to Computational Fluid Dynamics – The Finite Volume Method. Longman Scientific & Technical, Harlow, England.

Versteegh, T.A.M., Nieuwstadt, F.T.M., 1998. Turbulent budgets of natural convection in an infinite, differentially heated, vertical channel. International Journal of Heat and Fluid Flow 19, 135–149.